

Foiling Explanations in Deep Neural Networks

Snir Vitrack Tamam^{*1}, Raz Lapid^{*1,2}, and Moshe Sipper¹

¹Department of Computer Science, Ben-Gurion University, Beer Sheva 84105, Israel

²DeepKeep, Tel-Aviv, Israel

March 27, 2023

Abstract

Deep neural networks (DNNs) have greatly impacted numerous fields over the past decade. Yet despite exhibiting superb performance over many problems, their black-box nature still poses a significant challenge with respect to explainability. Indeed, explainable artificial intelligence (XAI) is crucial in several fields, wherein the answer alone—sans a reasoning of how said answer was derived—is of little value. This paper uncovers a troubling property of explanation methods for image-based DNNs: by making small visual changes to the input image—hardly influencing the network’s output—we demonstrate how explanations may be arbitrarily manipulated through the use of evolution strategies. Our novel algorithm, AttaXAI, a model-agnostic, adversarial attack on XAI algorithms, only requires access to the output logits of a classifier and to the explanation map; these weak assumptions render our approach highly useful where real-world models and data are concerned. We compare our method’s performance on two benchmark datasets—CIFAR100 and ImageNet—using four different pretrained deep-learning models: VGG16-CIFAR100, VGG16-ImageNet, MobileNet-CIFAR100, and Inception-v3-ImageNet. We find that the XAI methods can be manipulated without the use of gradients or other model internals. Our novel algorithm is successfully able to manipulate an image in a manner imperceptible to the human eye, such that the XAI method outputs a specific explanation map. To our knowledge, this is the first such method in a black-box setting, and we believe it has significant value where explainability is desired, required, or legally mandatory.

Keywords: deep learning, computer vision, adversarial attack, evolutionary algorithm, explainable artificial intelligence

1 Introduction

Recent research has revealed that deep learning-based, image-classification systems are vulnerable to adversarial instances, which are designed to deceive algorithms by introducing perturbations to benign images [4, 6, 14, 24, 48]. A variety of strategies have been developed to generate adversarial instances, and they fall under two broad categories, differing in the underlying threat model: white-box attacks [22, 27] and black-box attacks [5, 23].

In a white box attack, the attacker has access to the model’s parameters, including weights, gradients, etc’. In a black-box attack, the attacker has limited information or no

*Equal contribution

information at all; the attacker generates adversarial instances using either a different model, a model’s raw output (also called logits), or no model at all, the goal being for the result to transfer to the target model [18, 40].

In order to render a model more interpretable, various explainable algorithms have been conceived. Van Lent et al. [41] coined the term *Explainable Artificial Intelligence* (XAI), which refers to AI systems that “can explain their behavior either during execution or after the fact”. In-depth research into XAI methods has been sparked by the success of Machine Learning (ML) systems, particularly Deep Learning (DL), in a variety of domains, and the difficulty in intuitively understanding the outputs of complex models, namely, how did a DL model arrive at a specific decision for a given input.

Explanation techniques have drawn increased interest in recent years due to their potential to reveal hidden properties of deep neural networks [9]. For safety-critical applications, interpretability is essential, and sometimes even legally required.

The importance assigned to each input feature for the overall classification result may be observed through explanation maps, which can be used to offer explanations. Such maps can be used to create defenses and detectors for adversarial attacks [10, 19, 43]. Figures 1 and 2 show examples of explanation maps, generated by five different methods discussed in Section 2.

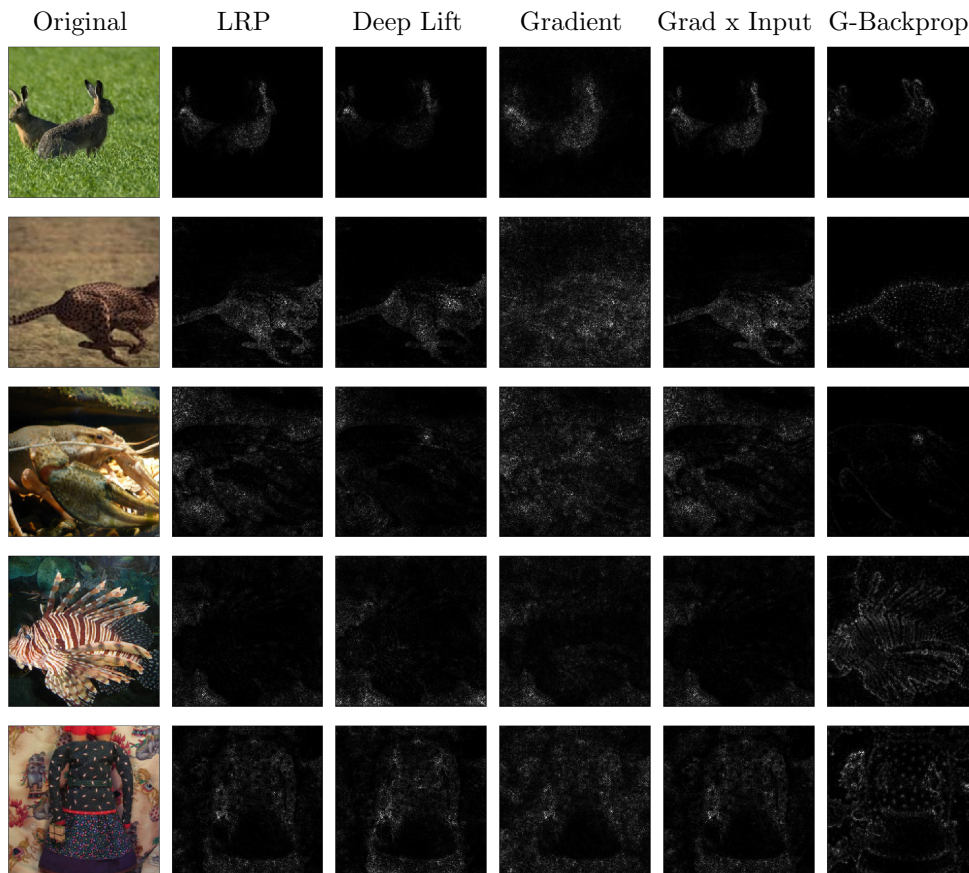


Figure 1: Explanation maps for 5 images using 5 different explanation methods. Dataset: ImageNet. Model: VGG16.

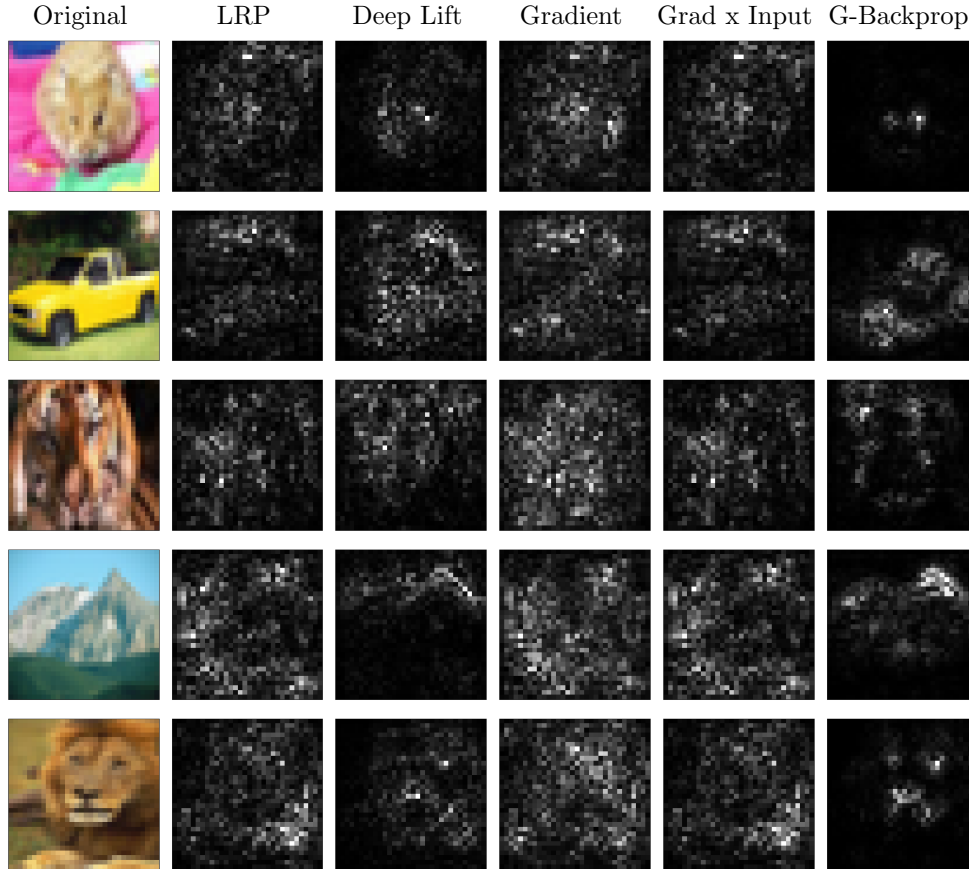


Figure 2: Explanation maps for 5 images using 5 different explanation methods. Dataset: CIFAR100. Model: VGG16.

In this paper, we show that these explanation maps can be transformed into any target map, using only the maps and the network’s output probability vector. This is accomplished by adding a perturbation to the input that is scarcely (if at all) noticeable to the human eye. This perturbation has minimal effect on the neural network’s output, therefore, in addition to the classification outcome, the probability vector of all classes remains virtually identical.

Our contribution. As we mentioned earlier, recent studies have shown that adversarial attacks may be used to undermine DNN predictions [4, 14, 23, 30]. There are several more papers regarding XAI attacks, which have also shown success on manipulating XAI, but to our knowledge, they all rely on access to the neural network’s gradient, which is usually not available in real-world scenarios [8, 11].

Herein, we propose a black-box algorithm, AttaXAI, which enables manipulation of an image through a barely noticeable perturbation, without the use of any model internals, such that the explanation fits any given target explanation. We study AttaXAI’s efficiency on 2 benchmark datasets, 4 different models, and 5 different XAI methods.

The next section presents related work. Section 3 presents AttaXAI, followed by experiments and results in Section 4. In Section 5 we discuss our results, followed by concluding remarks in Section 6.

2 Related Work

The ability of explanation maps to detect even the smallest visual changes was shown by Ghorbani et al. [11], where they perturbed a given image, which caused the explanatory map to change, without any specific target.

Kuppa and Le-Khac [21] designed a black-box attack to examine the security aspects of the gradient-based XAI approach, including consistency, accuracy, and confidence, using tabular datasets.

Zhang et al. [50] demonstrated a class of white-box attacks that provide adversarial inputs, which deceive both the interpretation models and the deep-learning models. They studied their method using four different explanation algorithms.

Xu et al. [48] demonstrated that a subtle adversarial perturbation intended to mislead classifiers might cause a significant change in a class-specific network interpretability map.

The goal of Dombrowski et al. [8] was to precisely replicate a given target map using gradient descent with respect to the input image. Although this work showed an intriguing phenomenon, it is a less-realistic scenario, since the attacker has full access to the targeted model.

We aimed to veer towards a more-realistic scenario and show that we can achieve similar results using no information about the model besides the probability output vector and the explanation map. To our knowledge, our work is the first to introduce a black-box attack on XAI gradient-based methods in the domain of image classification.

We will employ the following explanation techniques in this paper:

1. **Gradient:** Utilizing the saliency map, $g(x) = \frac{\partial f}{\partial x}(x)$, one may measure how small perturbations in each pixel alter the prediction of the model, $f(x)$ [36].
2. **Gradient \times Input:** The explanation map is calculated by multiplying the input by the partial derivatives of the output with regard to the input, $g(x) = \frac{\partial f}{\partial x}(x) \odot x$ [33].
3. **Guided Backpropagation:** A variant of the Gradient explanation, where the gradient's negative components are zeroed while backpropagating through the non-linearities of the model [37].
4. **Layer-wise Relevance Propagation (LRP):** With this technique, pixel importance propagates backwards across the network from top to bottom [1, 26]. The general propagation rule is the following:

$$R_j = \sum_k \frac{\alpha_j \rho(w_{jk})}{\epsilon + \sum_{0,j} \alpha_j \rho(w_{jk})} R_k, \tag{1}$$

where j and k are two neurons of any two consecutive layers, R_k, R_j are the relevance maps of layers k and j , respectively, ρ is a function that transforms the weights, and ϵ is a small positive increment.

In order to propagate relevance scores to the input layer (image pixels), the method applies an alternate propagation rule that properly handles pixel values received as input:

$$R_i = \sum_j \frac{\alpha_i w_{ij} - l_i w_{ij}^+ - h_i w_{ij}^-}{\sum_i \alpha_i w_{ij} - l_i w_{ij}^+ - h_i w_{ij}^-} R_j, \quad (2)$$

where l_i and h_i are the lower and upper bounds of pixel values.

5. **Deep Learning Important FeaTures (DeepLIFT)** compares a neuron’s activation to its “reference activation”, which then calculates contribution scores based on the difference. DeepLIFT has the potential to separately take into account positive and negative contributions, which might help to identify dependencies that other methods might have overlooked [34].

3 AttaXAI

This section presents our algorithm, AttaXAI, discussing first evolution strategies, and then delving into the algorithmic details.

3.1 Evolution Strategies

Our algorithm is based on Evolution Strategies (ES), a family of heuristic search techniques that draw their inspiration from natural evolution [2, 15]. Each iteration (aka generation) involves perturbing (through mutation) a population of vectors (genotypes) and assessing their objective function value (fitness value). The population of the next generation is created by combining the vectors with the highest fitness values, a process that is repeated until a stopping condition is met.

AttaXAI belongs to the class of Natural Evolution Strategies (NES) [13, 46], which includes several algorithms in the ES class that differ in the way they represent the population, and in their mutation and recombination operators. With NES, the population is represented as a distribution of parameter vectors, $\psi: p_\psi(\theta)$, which are each defined by a set of parameters, θ . By using stochastic gradient descent, NES attempts to maximize the population’s average fitness, $\mathbb{E}_{\theta \sim p_\psi}[f(\theta)]$, given a fitness function, $f(\theta)$.

A version of NES we found particularly useful for our case was used to solve common reinforcement learning (RL) problems [32]. In their study, a fitness function $f(\theta)$, where θ parameterizes the policy, captures the stochastic reward experienced over the course of an entire episode of agent interaction. The parameters $\theta_t^i \sim \mathcal{N}(\theta, \sigma^2 I)$ are taken from the population distribution p_{ψ_t} and evaluated to produce $f(\theta^i)$. θ_t is adjusted using an approximation of the gradient of the expected reward:

$$\nabla_\psi \mathbb{E}_{\theta \sim \psi}[f(\theta)] \approx \frac{1}{n} \sum_{i=1}^n f(\theta^i) \nabla_\psi \log p_\psi(\theta^i), \quad (3)$$

where n denotes how many samples were evaluated in each generation. The intuition behind NES is to sample parameters in the neighborhood of θ , and decide which direction θ should move to, such that the expected reward is increased.

Sampling from the population distribution is done by applying additive Gaussian noise to the current parameter vector: $\theta^i = \theta + \sigma \epsilon_i$, where $i \in [1, \dots, n]$ and $\epsilon_i \sim \mathcal{N}(0, I)$. The gradient is then approximated by calculating the weighted sum of sampled parameter perturbations by their rewards:

$$\nabla_{\theta} \mathbb{E}_{\epsilon \sim \mathcal{N}(0, I)} [f(\theta + \sigma \epsilon)] \approx \frac{1}{n\sigma} \sum_{i=1}^n f(\theta^i) \epsilon_i. \quad (4)$$

We use the strategy offered in [32] and rank-normalize $f(\theta^i)$ before obtaining the weighted sum. We update the time step parameter t via gradient ascent in the following manner:

$$\theta_{t+1} = \theta_t + \eta \nabla_{\theta_t} \mathbb{E}_{\epsilon \sim \mathcal{N}(0, I)} [f(\theta_t + \epsilon)], \quad (5)$$

where η is the learning learning rate.

Search Gradients. The core idea of Natural Evolution Strategies is to use search gradients to update the parameters of the search distribution [46]. The search gradient can be defined as the gradient of the expected fitness: Denoting by π a distribution with parameters θ , $\pi(z|\theta)$ is the probability density function of a given sample z . With $f(z)$ denoting the fitness of a sample z , the expected fitness under the search distribution can be written as:

$$J(\theta) = \mathbb{E}_{\theta} [f(z)] = \int f(z) \pi(z|\theta) dz. \quad (6)$$

The gradient with respect to the parameters can be expressed as:

$$\begin{aligned} \nabla_{\theta} J(\theta) &= \nabla_{\theta} \int f(z) \pi(z|\theta) dz \\ &= \int f(z) \nabla_{\theta} \pi(z|\theta) dz \\ &= \int f(z) \nabla_{\theta} \pi(z|\theta) \frac{\pi(z|\theta)}{\pi(z|\theta)} dz \\ &= \int [f(z) \nabla_{\theta} \log \pi(z|\theta)] \pi(z|\theta) dz \\ &= \mathbb{E}_{\theta} [f(z) \nabla_{\theta} \log \pi(z|\theta)] \end{aligned}$$

From these results we can approximate the gradient with Monte Carlo [25] samples $z_1, z_2, \dots, z_{\lambda}$:

$$\nabla_{\theta} J(\theta) \approx \frac{1}{\lambda} \sum_{k=1}^{\lambda} f(z_k) \nabla_{\theta} \log \pi(z_k|\theta).$$

In our experiment we sampled from a Gaussian distribution for calculating the search gradients. The parameter derivatives are [46]:

$$\begin{aligned} \nabla_{\mu} \log \mathcal{N}(\mu, \sigma) &= \frac{1}{\sigma^2} (z - \mu), \\ \nabla_{\sigma} \log \mathcal{N}(\mu, \sigma) &= \frac{(z - \mu)^2 - \sigma^2}{\sigma^3}. \end{aligned}$$

Latin Hypercube Sampling (LHS). LHS is a form of stratified sampling scheme, which improves the coverage of the sampling space. It is done by dividing a given cumulative distribution function into M non-overlapping intervals of equal y -axis length, and randomly choosing one value from each interval to obtain M samples. It ensures that each interval contains the same number of samples, thus producing good uniformity and symmetry [44]. We used both LHS and standard sampling in our experimental setup.

3.2 Algorithm

AttaXAI is an evolutionary algorithm (EA), which explores a space of images for adversarial instances that fool a given explanation method. This space of images is determined by a given input image, a model, and a loss function. The algorithm generates a perturbation for the given input image such that it fools the explanation method.

More formally, we consider a neural network, $f: \mathbb{R}^{h,w,c} \rightarrow \mathbb{R}^K$, which classifies a given image, $x \in \mathbb{R}^{h,w,c}$, where h, w, c are the image’s height, width, and channel count, respectively, to one of K predetermined categories, with the predicted class given by $k = \operatorname{argmax}_i f(x)_i$. The explanation map, which is represented by the function, $g: \mathbb{R}^{h,w,c} \rightarrow \mathbb{R}^{h,w}$, links each image to an explanation vector, of the same height and width, where each coordinate specifies the influence of each pixel on the network’s output.

AttaXAI explores the space of images through evolution, ultimately producing an adversarial image; it does so by continually updating a Gaussian probability distribution, used to sample the space of images. By continually improving this distribution the search improves.

We begin by sampling images from a normal distribution $\mathcal{N}(\mu, \sigma)$ centered around the original image x . Then we feed them to the model. By doing so, we can approximate the gradient of the expected fitness function. With an approximation of the gradient at hand we can advance in that direction by updating the search distribution parameters, μ and σ . A schematic of our algorithm is shown in Figure 3, with a full pseudocode provided in Algorithm 1.

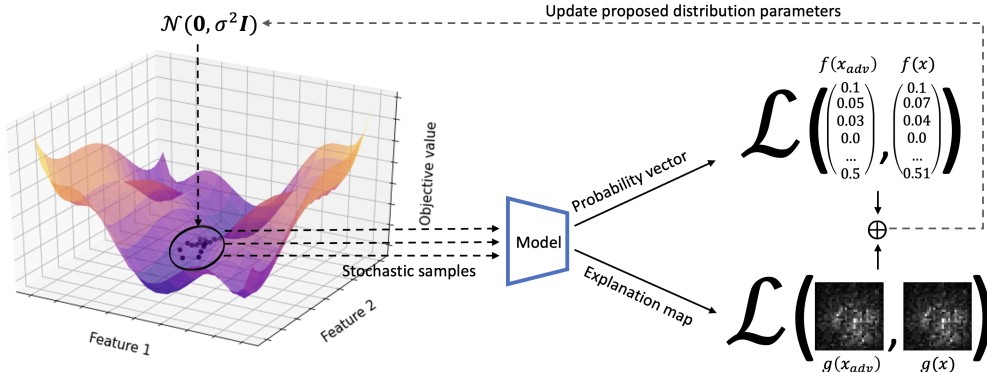


Figure 3: Schematic of proposed algorithm. Individual images are sampled from the population’s distribution $\mathcal{N}(\mu, \sigma)$, and fed into the model (Feature 1 and Feature 2 are image features, e.g., two pixel values; in reality the dimensionality is much higher). Then, the fitness function, i.e. the loss, is calculated using the output probability vectors and the explanation maps to approximate the gradient and update the distribution parameters, μ and σ .

3.3 Fitness Function

Given an image, $x \in \mathbb{R}^{h,w,c}$, a specific explanation method, $g: \mathbb{R}^{h,w,c} \rightarrow \mathbb{R}^{h,w}$, a target image, x_{target} , and a target explanation map, $g(x_{target})$, we seek an adversarial perturbation, $\delta \in \mathbb{R}^{h,w,c}$, such that the following properties of the adversarial instance, $x_{adv} = x + \delta$, hold:

1. The network’s prediction remains almost constant, i.e., $f(x) \approx f(x_{adv})$.

Algorithm 1 AttaXAI

Input:

$x \leftarrow$ original image
 $y \leftarrow$ original image's label
 $x_{expl} \leftarrow$ target explanation map
 $x_{pred} \leftarrow$ logits values of x
 $model \leftarrow$ model to be used
 $G \leftarrow$ maximum number of generations
 $\lambda \leftarrow$ population size
 $\sigma \leftarrow$ initial standard deviation value
 $\alpha \leftarrow$ explanation loss weight
 $\beta \leftarrow$ prediction loss weight
 $\eta_V \leftarrow$ attack vector learning rate
 $\eta_\sigma \leftarrow$ standard deviation learning rate

Output:

$\hat{x} \leftarrow$ adversarial image

```
# Main loop
1:  $\mu \leftarrow \mathbf{0}$  # mean remains constant throughout
2:  $V \leftarrow \vec{\mathbf{0}}$  # attack vector
3: for  $g = 1, 2, \dots, G$  do
4:   for  $k = 1, 2, \dots, \lambda$  do
5:     draw sample  $z_k \sim \mathcal{N}(\mu, \sigma^2)$  #  $z_k$  is used to perturb an image
6:     evaluate fitness  $f(z_k) = \text{FITNESS}(z_k)$ 
7:     calculate log-derivative  $\nabla_\mu \log \mathcal{N}(z_k | \mu, \sigma^2)$ 
8:     calculate log-derivative  $\nabla_\sigma \log \mathcal{N}(z_k | \mu, \sigma^2)$ 
9:      $\nabla_\mu J = \frac{1}{\lambda} \sum_{i=1}^\lambda f(z_k) \nabla_\mu \log \mathcal{N}(z_k | \mu, \sigma^2)$ 
10:     $\nabla_\sigma J = \frac{1}{\lambda} \sum_{i=1}^\lambda f(z_k) \nabla_\sigma \log \mathcal{N}(z_k | \mu, \sigma^2)$ 
11:     $V = V + \eta_V \cdot \nabla_\mu J$ 
12:     $\sigma = \sigma + \eta_\sigma \cdot \nabla_\sigma J$ 
13:  $\hat{x} = x + V$ 
14: function FITNESS( $z_k$ )
15:    $\hat{x} = x + V + z_k$ 
16:    $\hat{x}_{expl} = \text{XAI}(\hat{x}, y)$ 
17:    $\hat{x}_{pred} = \text{model}(\hat{x})$ 
18:    $expl_{loss} = \|x_{expl} - \hat{x}_{expl}\|_2^2$ 
19:    $pred_{loss} = \|x_{pred} - \hat{x}_{pred}\|_2^2$ 
20:   return  $\alpha * expl_{loss} + \beta * pred_{loss}$ 
```

2. The explanation vector of x_{adv} is close to the target explanation map, $g(x_{target})$, i.e., $g(x_{adv}) \approx g(x_{target})$.
3. The adversarial instance, x_{adv} , is close to the original image, x , i.e., $x \approx x_{adv}$.

We achieve such perturbations by optimizing the following fitness function of the evolutionary algorithm:

$$\mathcal{L} = \alpha \|g(x_{adv}) - g(x_{target})\| + \beta \|f(x_{adv}) - f(x)\| \quad (7)$$

The first term ensures that the altered explanation map, $g(x_{adv})$, is close to the target explanation map, $g(x_{target})$; the second term pushes the network to produce the same output probability vector. The hyperparameters, $\alpha, \beta \in \mathbb{R}^+$, determine the respective weightings of the fitness components.

We tried adding a third term to the fitness function, intended to minimize the mean squared error (MSE) distance between the perturbed image, x_{adv} , and the original, x , but this additional term did not improve results. We were able to achieve this goal by using a small amount of noise, whose value was multiplied by 0.999 every generation.

In order to use our approach, we only need the output probability vector, $f(x_{adv})$, and the target explanation map, $g(x_{target})$. Unlike white-box methods, we do not presuppose anything about the targeted model, its architecture, dataset, or training process. This makes our approach more realistic.

Minimizing the fitness value is the ultimate objective. Essentially, the value is better if the proper class’s logit remains the same and the explanation map looks similar to the targeted explanation map:

$$\operatorname{argmin}_{x_{adv}} \mathcal{L} = \alpha \|g(x_{adv}) - g(x_{target})\| + \beta \|f(x_{adv}) - f(x)\| \quad (8)$$

4 Experiments and Results

Assessing the algorithm over a particular configuration of model, dataset, and explanation technique, involves running it over 100 pairs of randomly selected images. We used 2 datasets: CIFAR100 and ImageNet [7]. For CIFAR100 we used the VGG16 [35] and MobileNet [17] models, and for ImageNet we used VGG16 and Inception [38]; the models are pretrained. For ImageNet, VGG16 has an accuracy of 73.3% and Inception-v3 has an accuracy of 78.8%. For CIFAR100, VGG16 has an accuracy of 72.9% and MobileNet has an accuracy of 69.0% (these are top-1 accuracy values; for ImageNet, top5 accuracy values are: VGG16 – 91.5%, Inception-v3 – 94.4%, and for CIFAR100, VGG16 – 91.2%, MobileNet – 91.0%). We chose these models because they are commonly used in the Computer Vision community for many downstream tasks [3, 16, 28, 42, 49].

The experimental setup is summarized in Algorithm 2: Choose 100 random image pairs from the given dataset. For each image pair compute a target explanation map, $g(x_{target})$, for one of the two images. With a budget of 50,000 queries to the model, Algorithm 1 perturbs the second image, aiming to replicate the desired $g(x_{target})$. We assume the model outputs both the output probability vector and the explanation map per each query to the model—which is a realistic scenario nowadays, with XAI algorithms being part of real-world applications [12, 31, 39].

We have two different weighting hyperparameters for the two datasets, which have been empirically proven to work: $\alpha = 1e11, \beta = 1e6$ for ImageNet, and $\alpha = 1e7, \beta = 1e6$ for CIFAR100. After every generation the learning rate was decreased through multiplication by a factor of 0.999. We tested drawing random samples, z_k , both independent and identically distributed (iid) and through Latin hypercube sampling (LHS). The generation of the explanations was achieved by using the repository Captum [20], a unified and generic model interpretability library for PyTorch.

Figures 4 through 7 shows samples of our results. Specifically, Figure 4 shows AttaXAI-generated attacks for images from ImageNet using the VGG16 model, against each of the 5 explanation methods: LRP, Deep Lift, Gradient, Gradient x Input, Guided-Backpropagation; Figure 5 shows AttaXAI-generated attacks for images from ImageNet using the Inception model; Figure 6 shows AttaXAI-generated attacks for images from CIFAR100 using the

Algorithm 2 Experimental setup (per dataset and model)

Input:

$dataset \leftarrow$ dataset to be used
 $model \leftarrow$ model to be used
 $G \leftarrow$ maximum number of generations
 $\lambda \leftarrow$ population size
 $\sigma \leftarrow$ initial standard deviation value
 $\alpha \leftarrow$ explanation-loss weight
 $\beta \leftarrow$ prediction-loss weight

Output:

Performance scores

- 1: **for** $i \leftarrow 1$ to 100 **do**
 - 2: Randomly choose a pair of images x and x_{target} from $dataset$
 - 3: Generate x_{adv} by running Algorithm 1, with x and x_{target} (and all other input parameters)
 - 4: Save performance statistics
-

VGG16 model; and Figure 7 shows AttaXAI-generated attacks for images from CIFAR100 using the MobileNet model.

Note that our primary objective has been achieved: having generated an adversarial image (x_{adv}), virtually identical to the original (x), the explanation (g) of the adversarial image (x_{adv}) is now, incorrectly, that of the target image (x_{target})—essentially, the two rightmost columns of Figures 4-7 are identical; furthermore, the class prediction remains the same, i.e., $\operatorname{argmax}_i f(x)_i = \operatorname{argmax}_i f(x_{adv})_i$.

5 Discussion

We examined the multitude of runs in-depth, producing several graphs, which are provided in full in the Appendix. Herein we summarize several observations we made:

- Our algorithm was successful in that $f(x_{adv}) \approx f(x)$ for all x_{adv} generated, and when applying argmax the original label remained unchanged.
- For most hyperparameter values examined, our approach converges for ImageNet using VGG, for every XAI except Guided Backpropagation (the latter likely able to be improved upon were we to increase the query budget).
- For all the experiments we witnessed that the Gradient XAI method showed the smallest mean squared error (MSE) between $g(x_{adv})$ and $g(x_{target})$, i.e., it was the least robust. The larger the MSE between $g(x_{adv})$ and $g(x_{target})$ the better the explanation algorithm can handle our perturbed image.
- For VGG16 (Figures 8 and 14), Gradient XAI showed the smallest median MSE between $g(x_{adv})$ and $g(x_{target})$, while Guided Backpropagation showed the most. This means that using Gradient XAI’s output as an explanation incurs the greatest risk, while using Guided Backpropagation’s output as an explanation incurs the smallest risk.

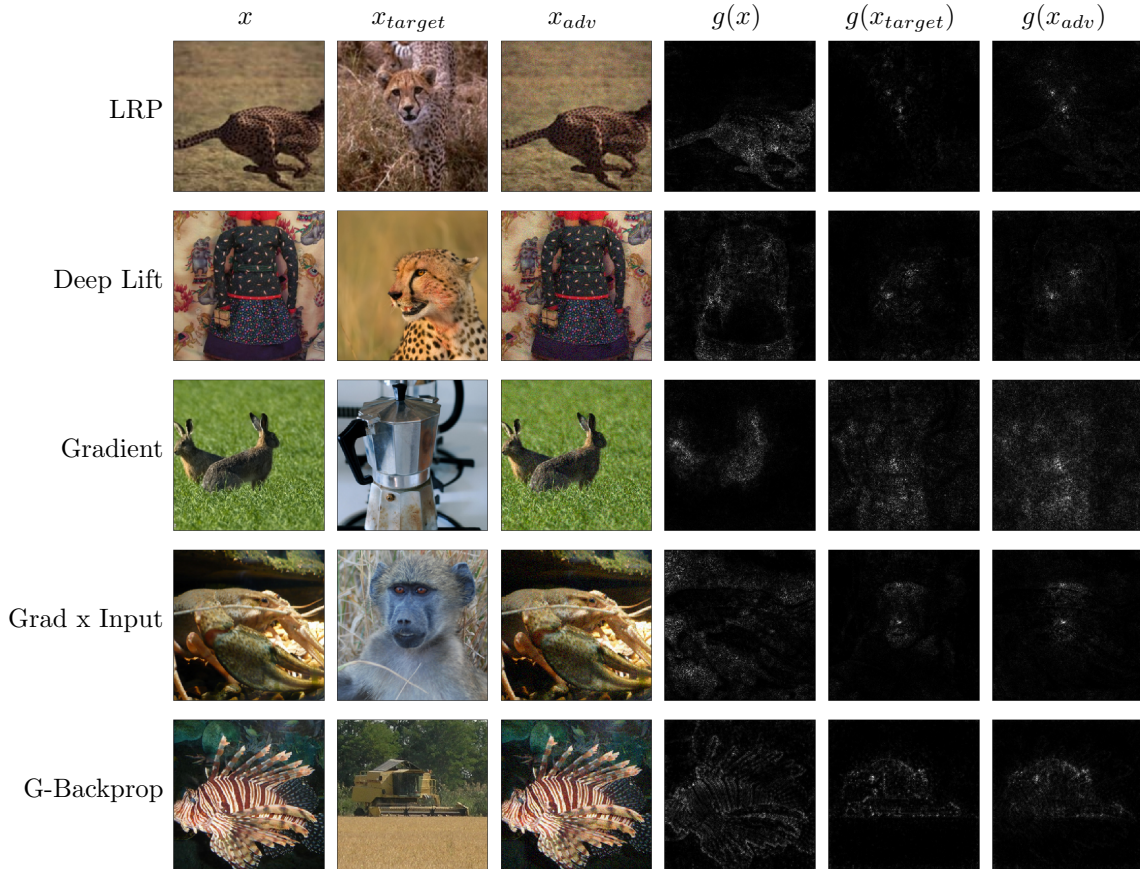


Figure 4: Attacks generated by AttaXAI. Dataset: ImageNet. Model: VGG16. Shown for the 5 explanation methods, described in the text: LRP, Deep Lift, Gradient, Gradient x Input, Guided Backpropagation (denoted G-Backprop in the figure). Note that our primary objective has been achieved: having generated an adversarial image (x_{adv}), virtually identical to the original (x), the explanation (g) of the adversarial image (x_{adv}) is now, incorrectly, that of the target image (x_{target}); essentially, the two rightmost columns are identical.

- For Inception (Figure 11), Gradient XAI and Guided Backpropagation exhibited the smallest median MSE, while LRP, Gradient x Input, and Deep Lift displayed similar results.
- For the MobileNet (Figure 17), Gradient XAI exhibited the smallest MSE, while Guided Backpropagation showed the largest MSE.
- MobileNet is more robust than VGG16 in that it attains lower MSE scores irrespective of the XAI method used. We surmise that this is due to the larger number of parameters in VGG16.
- The query budget was 50,000 for all experiments. In many runs the distance between the target explanation and the adversarial explanation reached a plateau after roughly 25,000 queries.

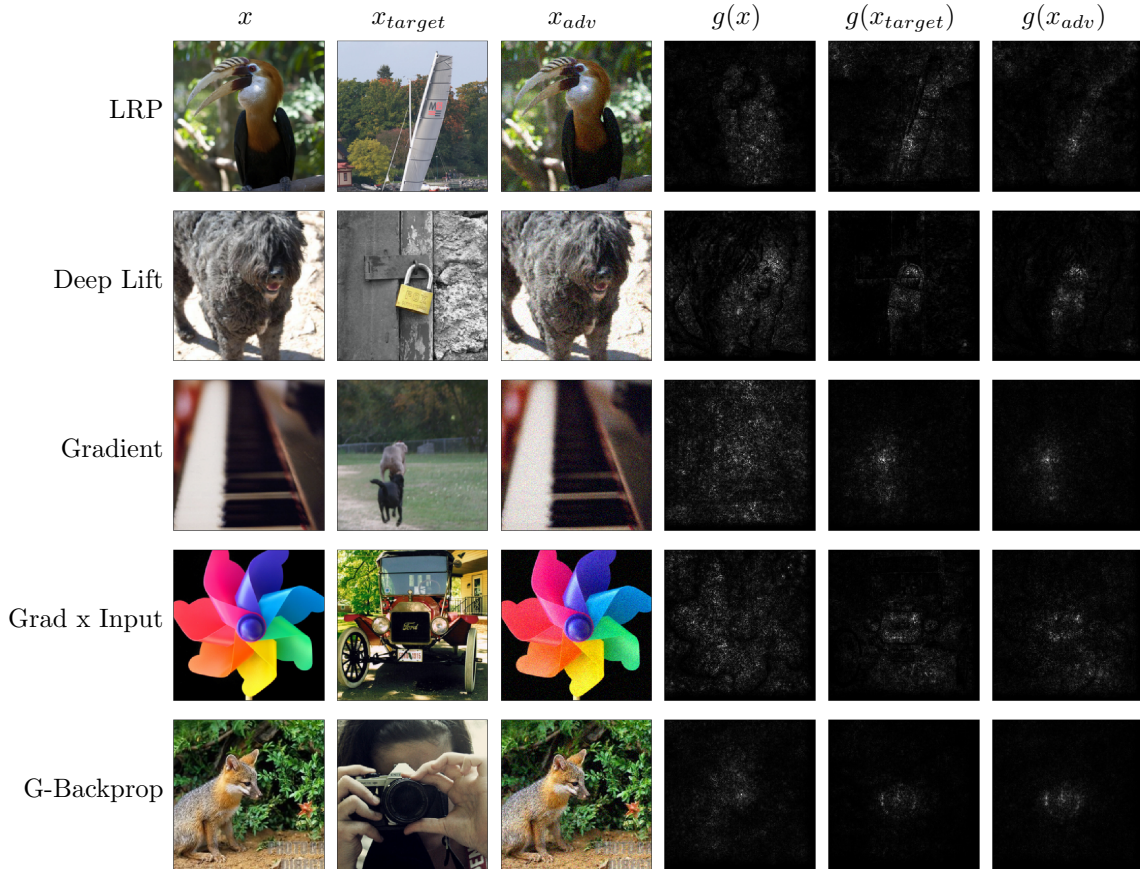


Figure 5: Attacks generated by AttaXAI. Dataset: ImageNet. Model: Inception.

6 Concluding Remarks

Recently, practitioners have started to use explanation approaches more frequently. We demonstrated how focused, undetectable modifications to the input data can result in arbitrary and significant adjustments to the explanation map. We showed that explanation maps of several known explanation algorithms may be modified at will. Importantly, this is feasible with a black-box approach, while maintaining the output of the model. We tested AttaXAI against the ImageNet and CIFAR100 datasets using 4 different network models.

XAI adversarial samples are hardly perceptible to the human eye. It is obvious that neural networks operate quite differently from humans, capturing fundamentally distinct properties. In addition, further work is required in the XAI domain to make XAI algorithms that are more reliable.

This work has shown that explanations are easily foiled—without any recourse to internal information—raising questions regarding XAI-based defenses and detectors.

Future Suggestions In our study we examined how to attack a model’s (XAI) explanation for a given input, prediction, and XAI method. Some questions still remain:

- A way to predict whether a XAI attack will be successful, and how many queries will be needed.

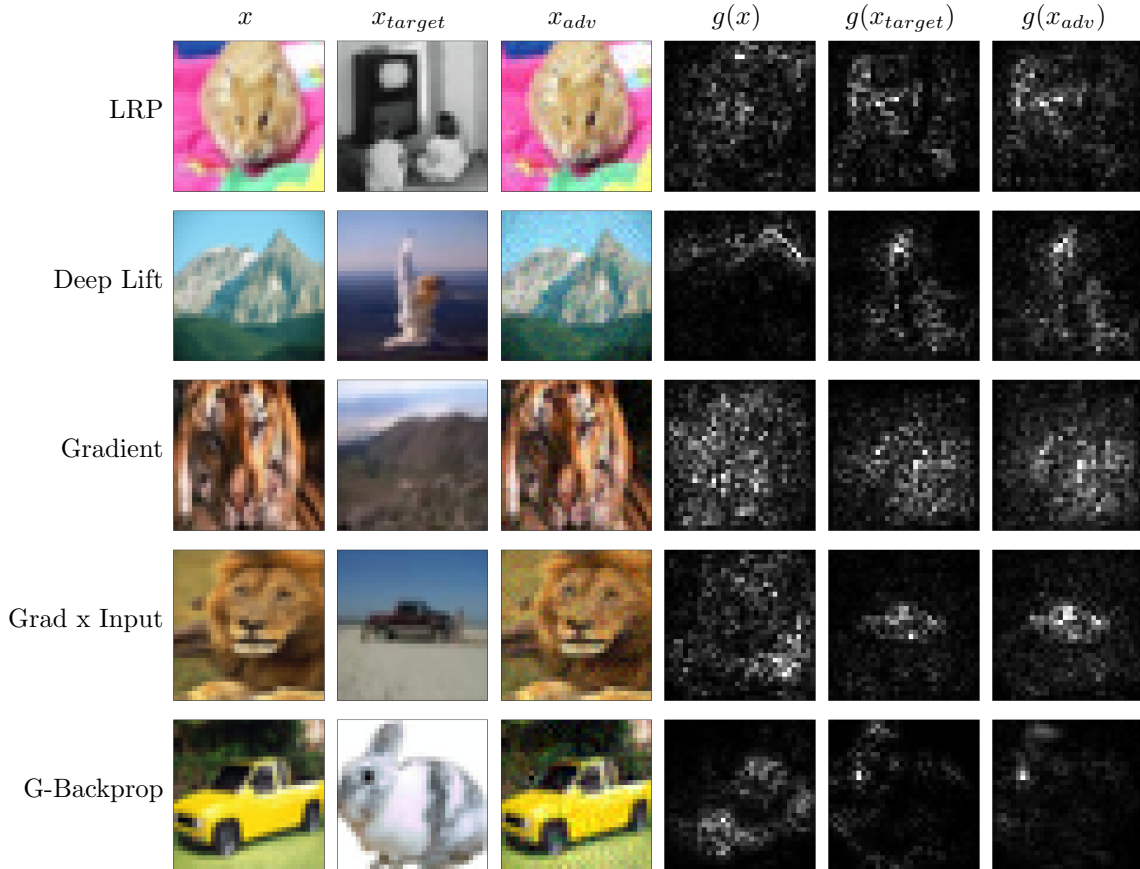


Figure 6: Attacks generated by AttaXAI. Dataset: CIFAR100. Model: VGG16.

- A better metric for a successful XAI attack, since in our results we observed that a smaller L2 distance does not necessarily translate to a more “convincing” attack. This problem is hard due to the non-objective nature of explanations.
- Find a way to eliminate the need for model feedback, i.e., go fully black-box. Applying XAI attacks via transferability [29, 45, 47] might be a way to move forward.
- When developing new XAI methods find ways to render them more robust to adversarial attacks.

Acknowledgement

This research was partially supported by the Israeli Innovation Authority through the Trust.AI consortium.

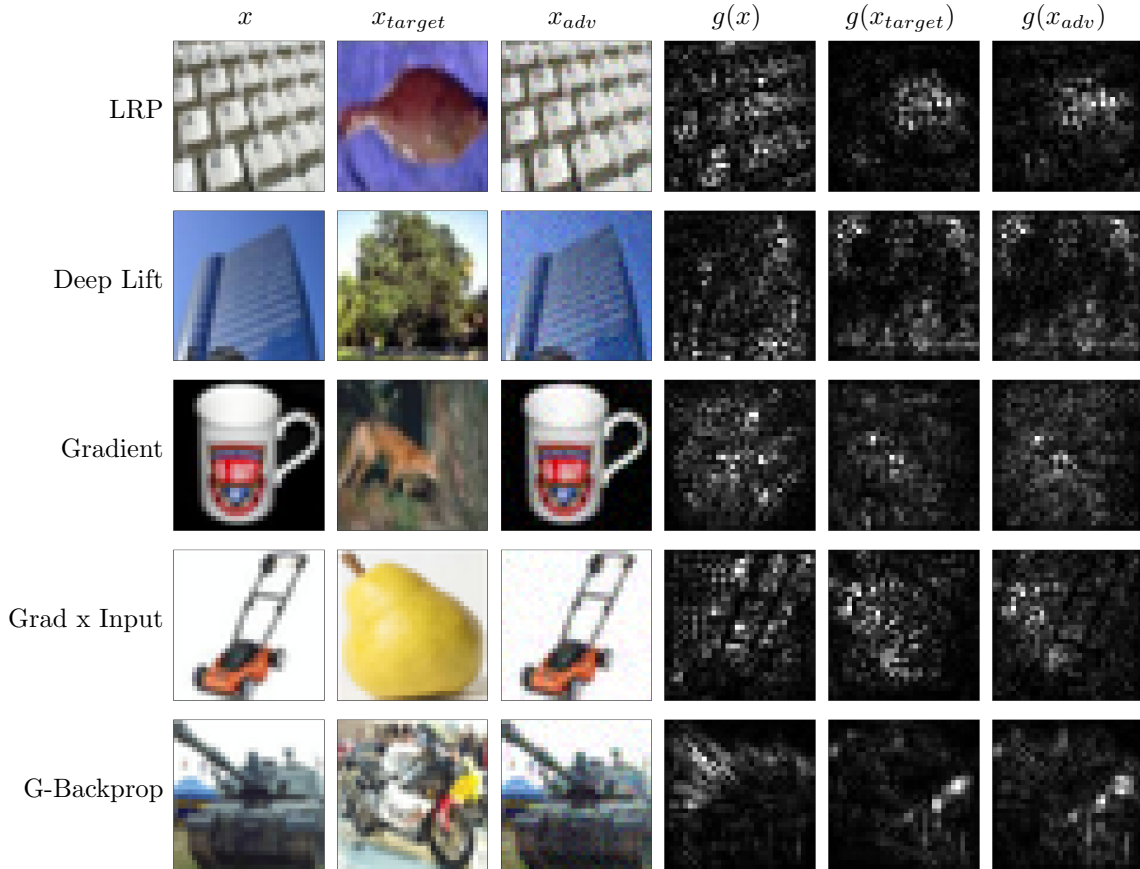


Figure 7: Attacks generated by AttaXAI. Dataset: CIFAR100. Model: MobileNet.

References

- [1] S. Bach, A. Binder, G. Montavon, F. Klauschen, K.-R. Müller, and W. Samek. On pixel-wise explanations for non-linear classifier decisions by layer-wise relevance propagation. *PLoS One*, 10(7):e0130140, 2015.
- [2] H.-G. Beyer and H.-P. Schwefel. Evolution strategies—a comprehensive introduction. *Natural Computing*, 1(1):3–52, 2002.
- [3] Y. Bhatia, A. Bajpayee, D. Raghuvanshi, and H. Mittal. Image captioning using Google’s Inception-Resnet-v2 and recurrent neural network. In *2019 Twelfth International Conference on Contemporary Computing (IC3)*, pages 1–6. IEEE, 2019.
- [4] N. Carlini and D. Wagner. Towards evaluating the robustness of neural networks. In *2017 IEEE Symposium on Security and Privacy (SP)*, pages 39–57. IEEE, 2017.
- [5] P.-Y. Chen, H. Zhang, Y. Sharma, J. Yi, and C.-J. Hsieh. Zoo: Zeroth order optimization based black-box attacks to deep neural networks without training substitute models. In *Proceedings of the 10th ACM Workshop on Artificial Intelligence and Security*, pages 15–26, 2017.

- [6] F. Croce and M. Hein. Reliable evaluation of adversarial robustness with an ensemble of diverse parameter-free attacks. In *International Conference on Machine Learning*, pages 2206–2216. PMLR, 2020.
- [7] J. Deng, W. Dong, R. Socher, L.-J. Li, K. Li, and L. Fei-Fei. Imagenet: A large-scale hierarchical image database. In *2009 IEEE Conference on Computer Vision and Pattern Recognition*, pages 248–255. IEEE, 2009.
- [8] A.-K. Dombrowski, M. Alber, C. Anders, M. Ackermann, K.-R. Müller, and P. Kessel. Explanations can be manipulated and geometry is to blame. *Advances in Neural Information Processing Systems*, 32, 2019.
- [9] F. K. Došilović, M. Brčić, and N. Hlupić. Explainable artificial intelligence: A survey. In *2018 41st International Convention on Information and Communication Technology, Electronics and Microelectronics (MIPRO)*, pages 0210–0215. IEEE, 2018.
- [10] G. Fidel, R. Bitton, and A. Shabtai. When explainability meets adversarial learning: Detecting adversarial examples using shap signatures. In *2020 International Joint Conference on Neural Networks (IJCNN)*, pages 1–8. IEEE, 2020.
- [11] A. Ghorbani, A. Abid, and J. Zou. Interpretation of neural networks is fragile. In *Proceedings of the AAAI Conference on Artificial Intelligence*, volume 33, pages 3681–3688, 2019.
- [12] F. Giuste, W. Shi, Y. Zhu, T. Naren, M. Isgut, Y. Sha, L. Tong, M. Gupte, and M. D. Wang. Explainable artificial intelligence methods in combating pandemics: A systematic review. *IEEE Reviews in Biomedical Engineering*, 2022.
- [13] T. Glasmachers, T. Schaul, S. Yi, D. Wierstra, and J. Schmidhuber. Exponential natural evolution strategies. In *Proceedings of the 12th Annual Conference on Genetic and Evolutionary Computation*, pages 393–400, 2010.
- [14] I. J. Goodfellow, J. Shlens, and C. Szegedy. Explaining and harnessing adversarial examples. *arXiv preprint arXiv:1412.6572*, 2014.
- [15] N. Hansen, D. V. Arnold, and A. Auger. Evolution strategies. In *Springer Handbook of Computational Intelligence*, pages 871–898. Springer, 2015.
- [16] M. F. Haque, H.-Y. Lim, and D.-S. Kang. Object detection based on vgg with resnet network. In *2019 International Conference on Electronics, Information, and Communication (ICEIC)*, pages 1–3. IEEE, 2019.
- [17] A. G. Howard, M. Zhu, B. Chen, D. Kalenichenko, W. Wang, T. Weyand, M. Andreetto, and H. Adam. Mobilenets: Efficient convolutional neural networks for mobile vision applications. *arXiv preprint arXiv:1704.04861*, 2017.
- [18] N. Inkawhich, W. Wen, H. H. Li, and Y. Chen. Feature space perturbations yield more transferable adversarial examples. In *Proceedings of the IEEE/CVF Conference on Computer Vision and Pattern Recognition*, pages 7066–7074, 2019.

- [19] C.-Y. Kao, J. Chen, K. Markert, and K. Böttinger. Rectifying adversarial inputs using xai techniques. In *2022 30th European Signal Processing Conference (EUSIPCO)*, pages 573–577. IEEE, 2022.
- [20] N. Kokhlikyan, V. Miglani, M. Martin, E. Wang, B. Alsallakh, J. Reynolds, A. Melnikov, N. Kliushkina, C. Araya, S. Yan, and O. Reblitz-Richardson. Captum: A unified and generic model interpretability library for pytorch, 2020.
- [21] A. Kuppa and N.-A. Le-Khac. Black box attacks on explainable artificial intelligence (xai) methods in cyber security. In *2020 International Joint Conference on Neural Networks (IJCNN)*, pages 1–8. IEEE, 2020.
- [22] A. Kurakin, I. J. Goodfellow, and S. Bengio. Adversarial examples in the physical world. In *Artificial Intelligence Safety and Security*, pages 99–112. Chapman and Hall/CRC, 2018.
- [23] R. Lapid, Z. Haramaty, and M. Sipper. An evolutionary, gradient-free, query-efficient, black-box algorithm for generating adversarial instances in deep convolutional neural networks. *Algorithms*, 15(11), 2022.
- [24] A. Madry, A. Makelov, L. Schmidt, D. Tsipras, and A. Vladu. Towards deep learning models resistant to adversarial attacks. *arXiv preprint arXiv:1706.06083*, 2017.
- [25] N. Metropolis and S. Ulam. The Monte Carlo method. *Journal of the American Statistical Association*, 44(247):335–341, 1949.
- [26] G. Montavon, A. Binder, S. Lapuschkin, W. Samek, and K.-R. Müller. Layer-wise relevance propagation: an overview. *Explainable AI: interpreting, explaining and visualizing deep learning*, pages 193–209, 2019.
- [27] S.-M. Moosavi-Dezfooli, A. Fawzi, and P. Frossard. Deepfool: a simple and accurate method to fool deep neural networks. In *Proceedings of the IEEE conference on computer vision and pattern recognition*, pages 2574–2582, 2016.
- [28] C. Ning, H. Zhou, Y. Song, and J. Tang. Inception single shot multibox detector for object detection. In *2017 IEEE International Conference on Multimedia & Expo Workshops (ICMEW)*, pages 549–554. IEEE, 2017.
- [29] N. Papernot, P. McDaniel, and I. Goodfellow. Transferability in machine learning: from phenomena to black-box attacks using adversarial samples. *arXiv preprint arXiv:1605.07277*, 2016.
- [30] N. Papernot, P. McDaniel, S. Jha, M. Fredrikson, Z. B. Celik, and A. Swami. The limitations of deep learning in adversarial settings. In *2016 IEEE European Symposium on Security and Privacy (EuroSecP)*, pages 372–387. IEEE, 2016.
- [31] S. N. Payrovnaziri, Z. Chen, P. Rengifo-Moreno, T. Miller, J. Bian, J. H. Chen, X. Liu, and Z. He. Explainable artificial intelligence models using real-world electronic health record data: a systematic scoping review. *Journal of the American Medical Informatics Association*, 27(7):1173–1185, 2020.

- [32] T. Salimans, J. Ho, X. Chen, S. Sidor, and I. Sutskever. Evolution strategies as a scalable alternative to reinforcement learning. *arXiv preprint arXiv:1703.03864*, 2017.
- [33] A. Shrikumar, P. Greenside, A. Shcherbina, and A. Kundaje. Not just a black box: Learning important features through propagating activation differences. *arXiv preprint arXiv:1605.01713*, 2016.
- [34] A. Shrikumar, P. Greenside, and A. Kundaje. Learning important features through propagating activation differences. In *International Conference on Machine Learning*, pages 3145–3153. PMLR, 2017.
- [35] K. Simonyan and A. Zisserman. Very deep convolutional networks for large-scale image recognition. *arXiv preprint arXiv:1409.1556*, 2014.
- [36] K. Simonyan, A. Vedaldi, and A. Zisserman. Deep inside convolutional networks: Visualising image classification models and saliency maps. *arXiv preprint arXiv:1312.6034*, 2013.
- [37] J. T. Springenberg, A. Dosovitskiy, T. Brox, and M. Riedmiller. Striving for simplicity: The all convolutional net. *arXiv preprint arXiv:1412.6806*, 2014.
- [38] C. Szegedy, W. Liu, Y. Jia, P. Sermanet, S. Reed, D. Anguelov, D. Erhan, V. Vanhoucke, and A. Rabinovich. Going deeper with convolutions. In *Proceedings of the IEEE Conference on Computer Vision and Pattern Recognition*, pages 1–9, 2015.
- [39] E. Tjoa and C. Guan. A survey on explainable artificial intelligence (xai): Toward medical xai. *IEEE Transactions on Neural Networks and Learning Systems*, 32(11):4793–4813, 2020.
- [40] F. Tramèr, N. Papernot, I. Goodfellow, D. Boneh, and P. McDaniel. The space of transferable adversarial examples. *arXiv preprint arXiv:1704.03453*, 2017.
- [41] M. Van Lent, W. Fisher, and M. Mancuso. An explainable artificial intelligence system for small-unit tactical behavior. In *Proceedings of the National Conference on Artificial Intelligence*, pages 900–907. Menlo Park, CA; Cambridge, MA; London; AAAI Press; MIT Press; 1999, 2004.
- [42] I. B. Venkateswarlu, J. Kakarla, and S. Prakash. Face mask detection using mobilenet and global pooling block. In *2020 IEEE 4th Conference on Information & Communication Technology (CICT)*, pages 1–5. IEEE, 2020.
- [43] S. Walia, K. Kumar, S. Agarwal, and H. Kim. Using xai for deep learning-based image manipulation detection with shapley additive explanation. *Symmetry*, 14(8):1611, 2022.
- [44] D. Wang, J. Lin, and Y.-G. Wang. Query-efficient adversarial attack based on latin hypercube sampling. *arXiv preprint arXiv:2207.02391*, 2022.
- [45] X. Wang, X. He, J. Wang, and K. He. Admix: Enhancing the transferability of adversarial attacks. In *Proceedings of the IEEE/CVF International Conference on Computer Vision*, pages 16158–16167, 2021.

- [46] D. Wierstra, T. Schaul, T. Glasmachers, Y. Sun, J. Peters, and J. Schmidhuber. Natural evolution strategies. *Journal of Machine Learning Research*, 15(1):949–980, 2014.
- [47] C. Xie, Z. Zhang, Y. Zhou, S. Bai, J. Wang, Z. Ren, and A. L. Yuille. Improving transferability of adversarial examples with input diversity. In *Proceedings of the IEEE/CVF Conference on Computer Vision and Pattern Recognition*, pages 2730–2739, 2019.
- [48] K. Xu, S. Liu, P. Zhao, P.-Y. Chen, H. Zhang, Q. Fan, D. Erdogmus, Y. Wang, and X. Lin. Structured adversarial attack: Towards general implementation and better interpretability. *arXiv preprint arXiv:1808.01664*, 2018.
- [49] A. Younis, L. Shixin, S. Jn, and Z. Hai. Real-time object detection using pre-trained deep learning models MobileNet-SSD. In *Proceedings of 2020 the 6th International Conference on Computing and Data Engineering*, pages 44–48, 2020.
- [50] X. Zhang, N. Wang, H. Shen, S. Ji, X. Luo, and T. Wang. Interpretable deep learning under fire. In *29th {USENIX} Security Symposium ({USENIX} Security 20)*, 2020.

Appendix

The following figures provide our full qualitative results. Hyperparameters: n_pop – population size of evolutionary algorithm; lr – learning rate of gradient approximation step for updating the attack; LS – use of Latin sampling or regular sampling.

- Figure 8: Similarity in terms of MSE between the target explanation map, $g(x_{target})$, and the best final adversarial explanation map, $g(x_{adv})$, for 8 different hyperparameter configurations (dataset: ImageNet, model: VGG16).
- Figure 9: Similarity in terms of MSE between the input image, x , and the best final adversarial, x_{adv} , for 8 different hyperparameter configurations (dataset: ImageNet, model: VGG16).
- Figure 10: MSE loss value as function of evolutionary generation for 8 different hyperparameter configurations (dataset: ImageNet, model: VGG16).
- Figure 11: Similarity in terms of MSE between the target explanation map, $g(x_{target})$, and the best final adversarial explanation map, $g(x_{adv})$, for 8 different hyperparameter configurations (dataset: ImageNet, model: Inception).
- Figure 12: MSE loss values for the input image versus the chosen adversarial image for 8 different hyperparameter configurations (dataset: ImageNet, model: Inception).
- Figure 13: MSE loss value as function of evolutionary generation for 8 different hyperparameter configurations (dataset: ImageNet, model: Inception).
- Figure 14: Similarity in terms of MSE between the target explanation map, $g(x_{target})$, and the best final adversarial explanation map, $g(x_{adv})$, for 8 different hyperparameter configurations (dataset: CIFAR100, model: VGG16).
- Figure 15: MSE loss value for input image versus chosen adversarial image for 8 different hyperparameter configurations (dataset: CIFAR100, model: VGG16).
- Figure 16: MSE loss value as function of evolutionary generation for 8 different hyperparameter configurations (dataset: CIFAR100, model: VGG16).
- Figure 17: Similarity in terms of MSE between the target explanation map, $g(x_{target})$, and the best final adversarial explanation map, $g(x_{adv})$, for 8 different hyperparameter configurations (dataset: CIFAR100, model: MobileNet).
- Figure 18: MSE loss value for input image versus chosen adversarial image for 8 different hyperparameter configurations (dataset: CIFAR100, model: MobileNet).
- Figure 19: MSE loss value as function of evolutionary generation for 8 different hyperparameter configurations (dataset: CIFAR100, model: MobileNet).

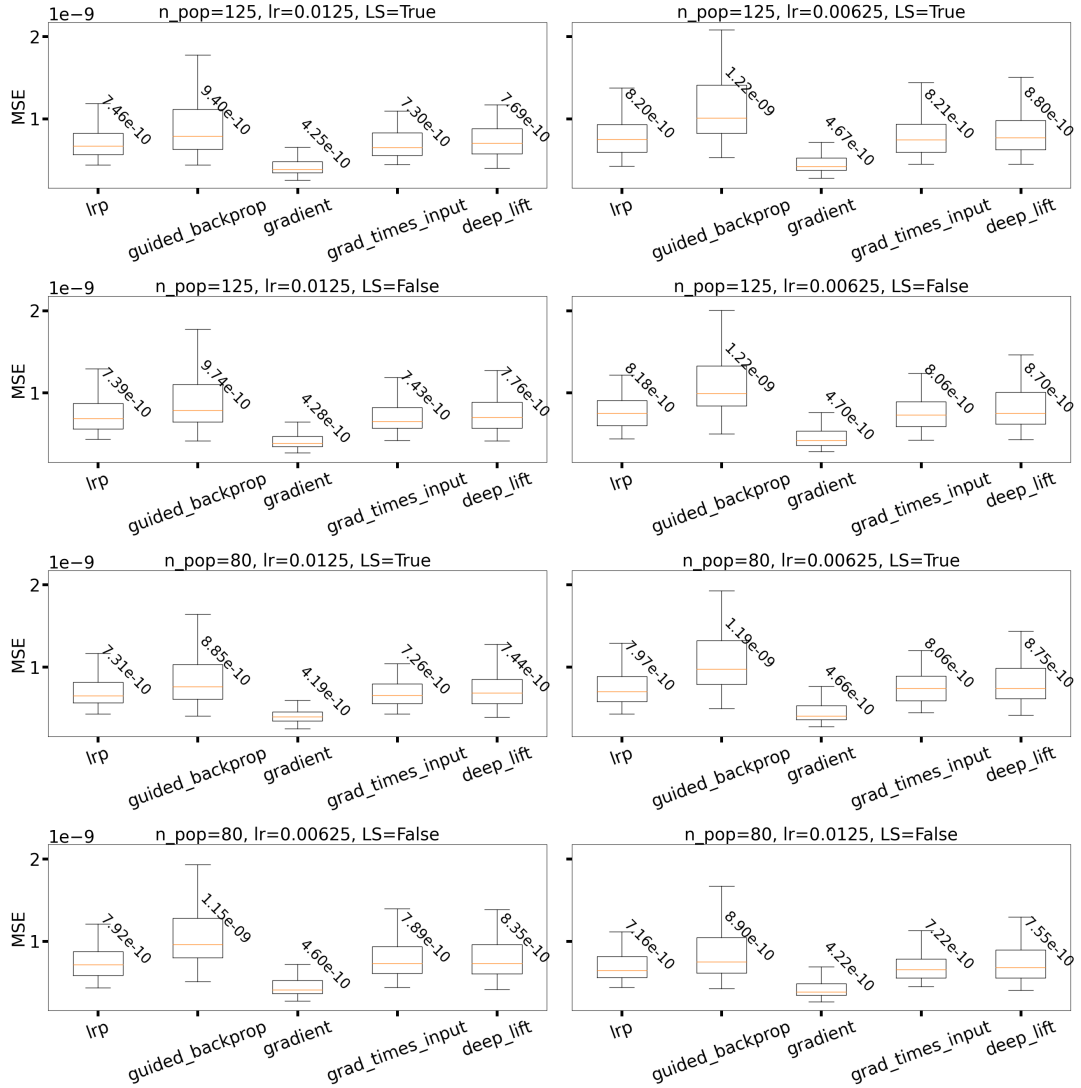


Figure 8: Similarity in terms of MSE between target explanation map, $g(x_{target})$, and best final adversarial explanation map, $g(x_{adv})$, for 8 different hyperparameter configurations. Dataset: ImageNet. Model: VGG16. The Gradient XAI method is the most susceptible to attacks while Guided backpropogation is the hardest to attack; Deep Lift, LRP, and Gradient x Input are similar.

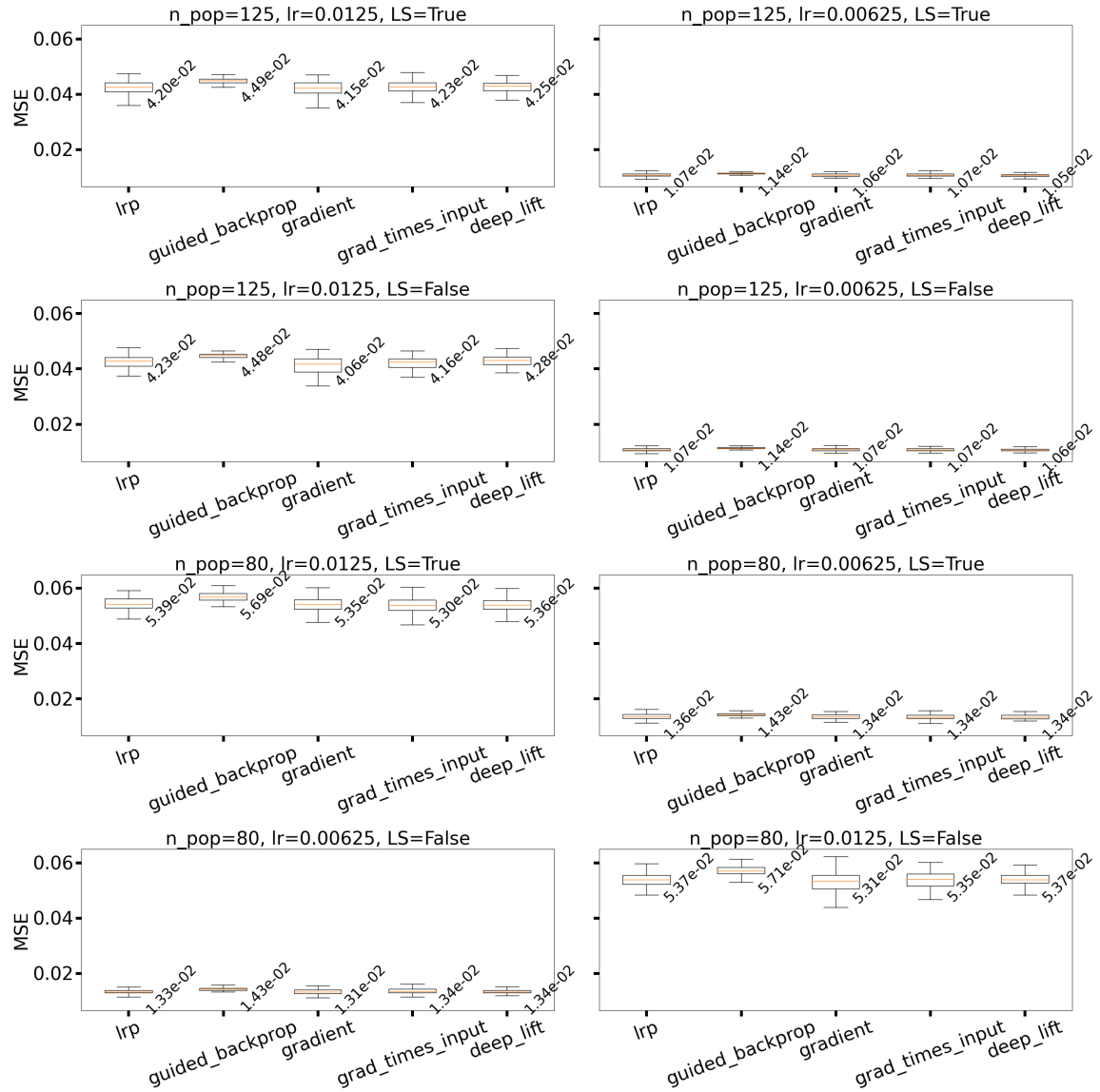


Figure 9: Similarity in terms of MSE between input image, x , and best final adversarial, x_{adv} , for 8 different hyperparameter configurations. Dataset: ImageNet. Model: VGG16. A higher learning rate and a smaller population size (i.e., more gradient steps) contribute to the perturbation of the image. The sampling method has no effect.

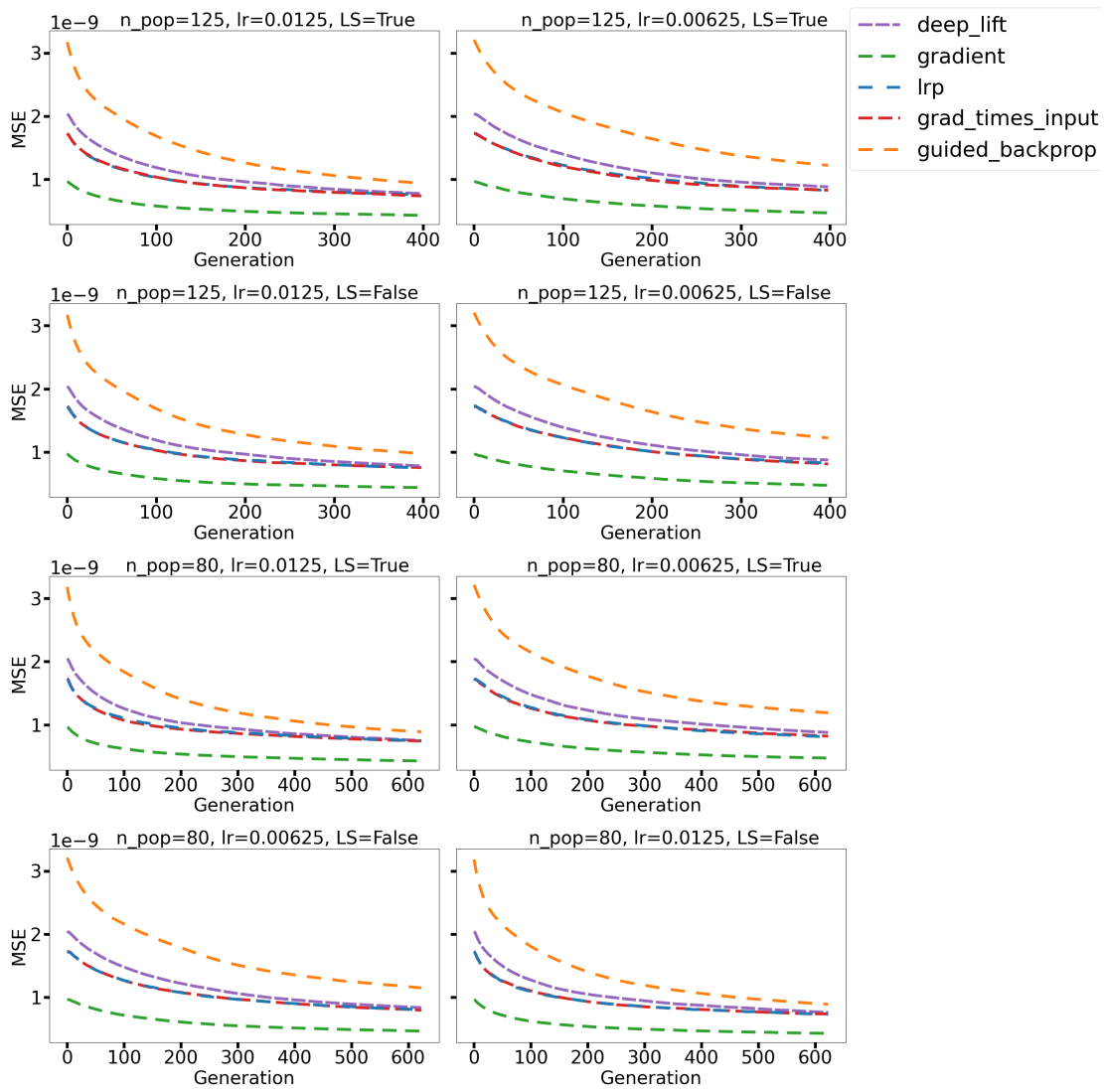


Figure 10: MSE loss value as function of evolutionary generation for 8 different hyperparameter configurations. Dataset: ImageNet. Model: VGG16.

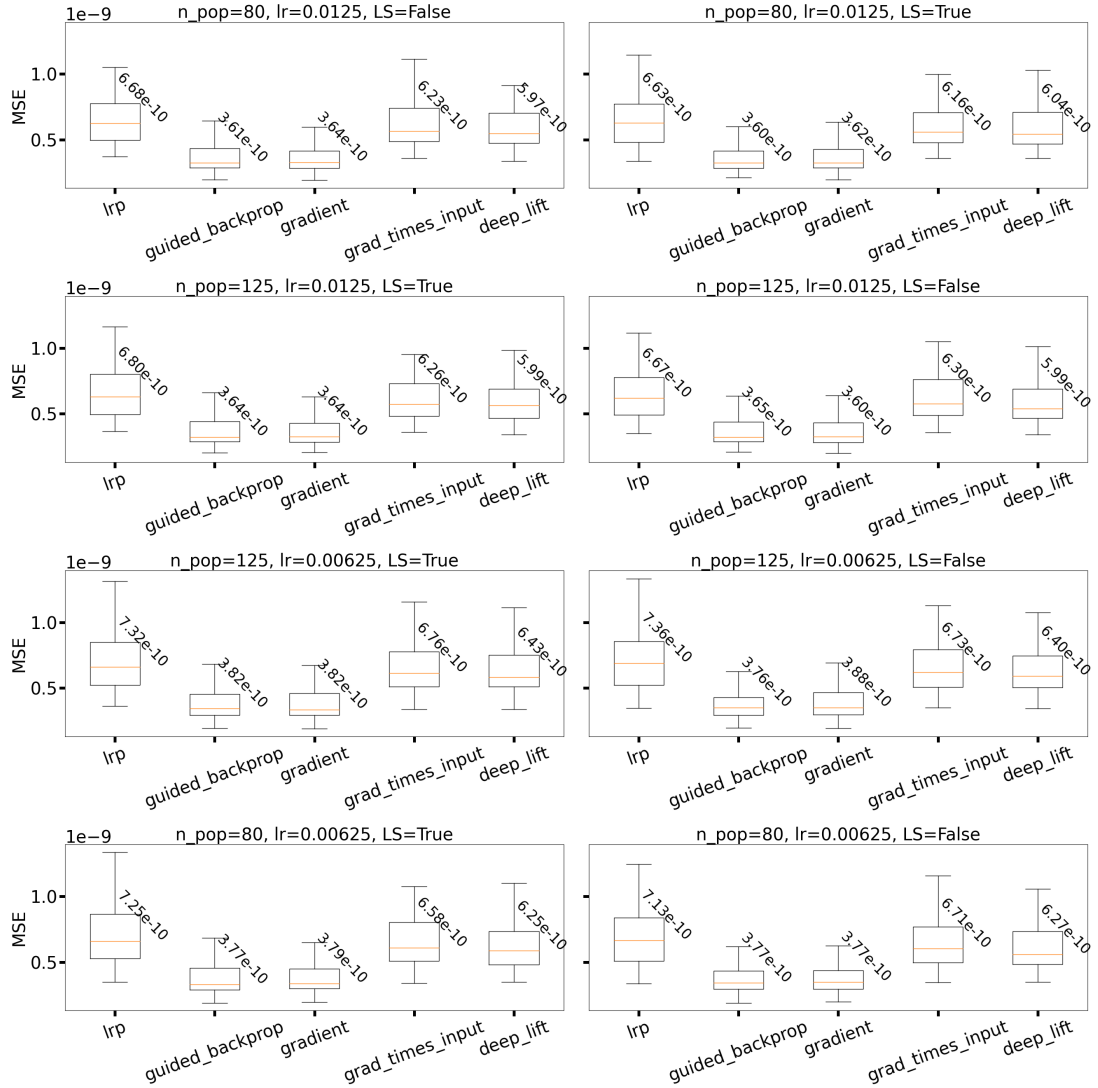


Figure 11: Similarity in terms of MSE between target explanation map, $g(x_{target})$, and best final adversarial explanation map, $g(x_{adv})$, for 8 different hyperparameter configurations. Dataset: ImageNet. Model: Inception. The Gradient XAI and Guided backpropogation methods are the most susceptible to attacks while Deep Lift, LRP, and Gradient x Input are less susceptible.

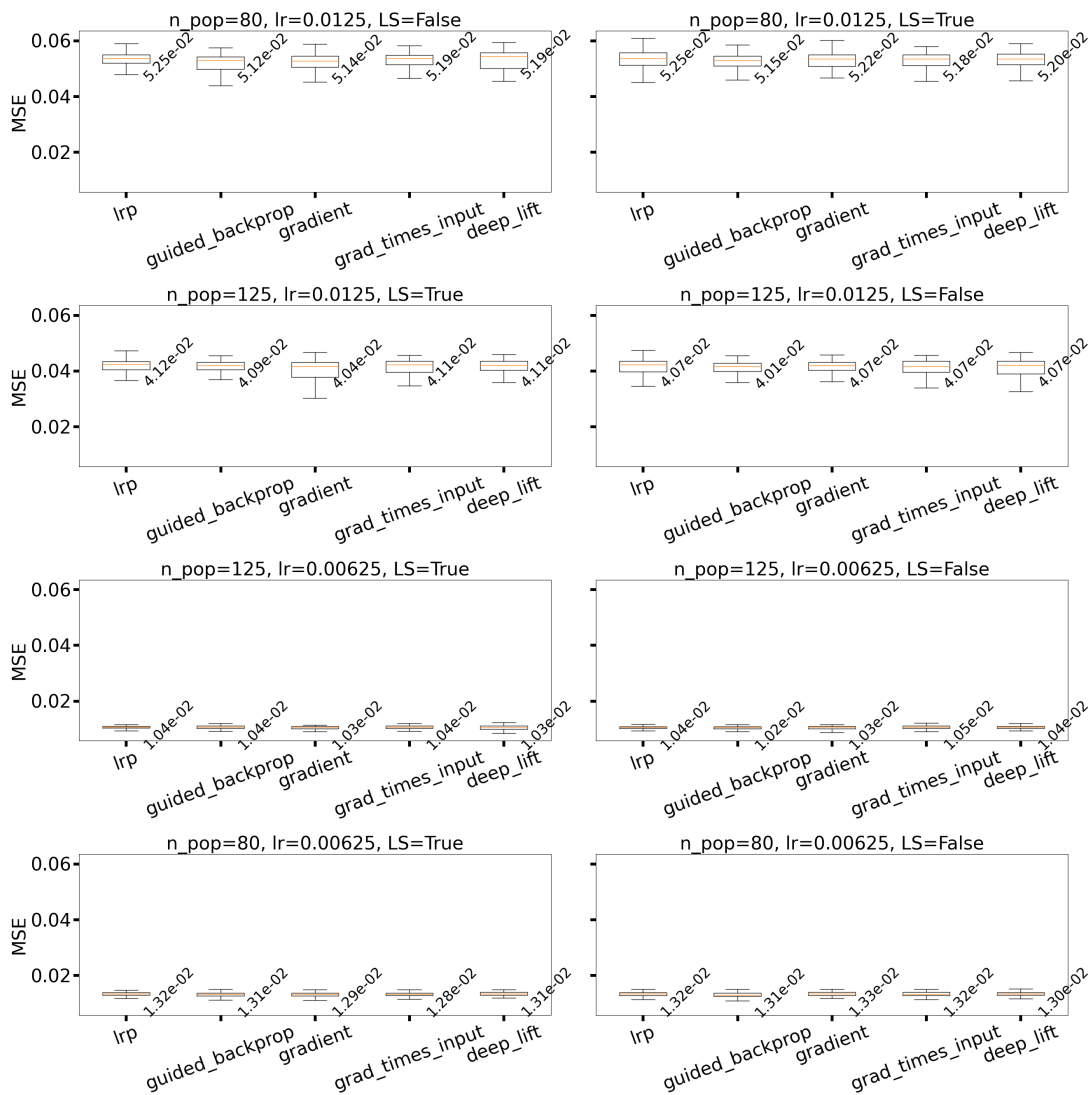


Figure 12: MSE loss value for input image versus chosen adversarial image for 8 different hyperparameter configurations. Dataset: ImageNet. Model: Inception. A higher learning rate and a smaller population size (i.e., more gradient steps) contribute to the perturbation of the image. The sampling method has no effect.

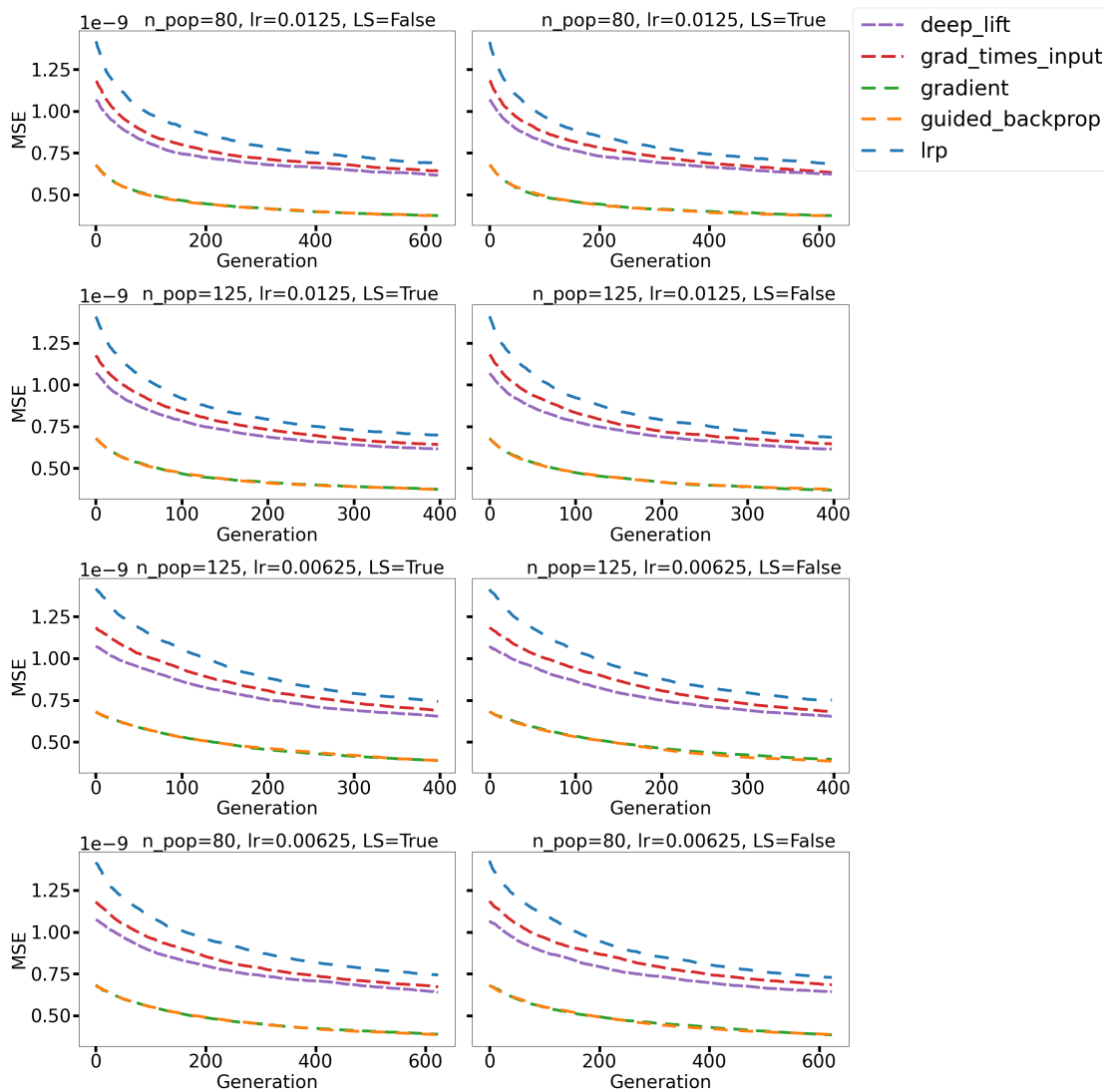


Figure 13: MSE loss value as function of evolutionary generation for 8 different hyperparameter configurations. Dataset: ImageNet. Model: Inception.

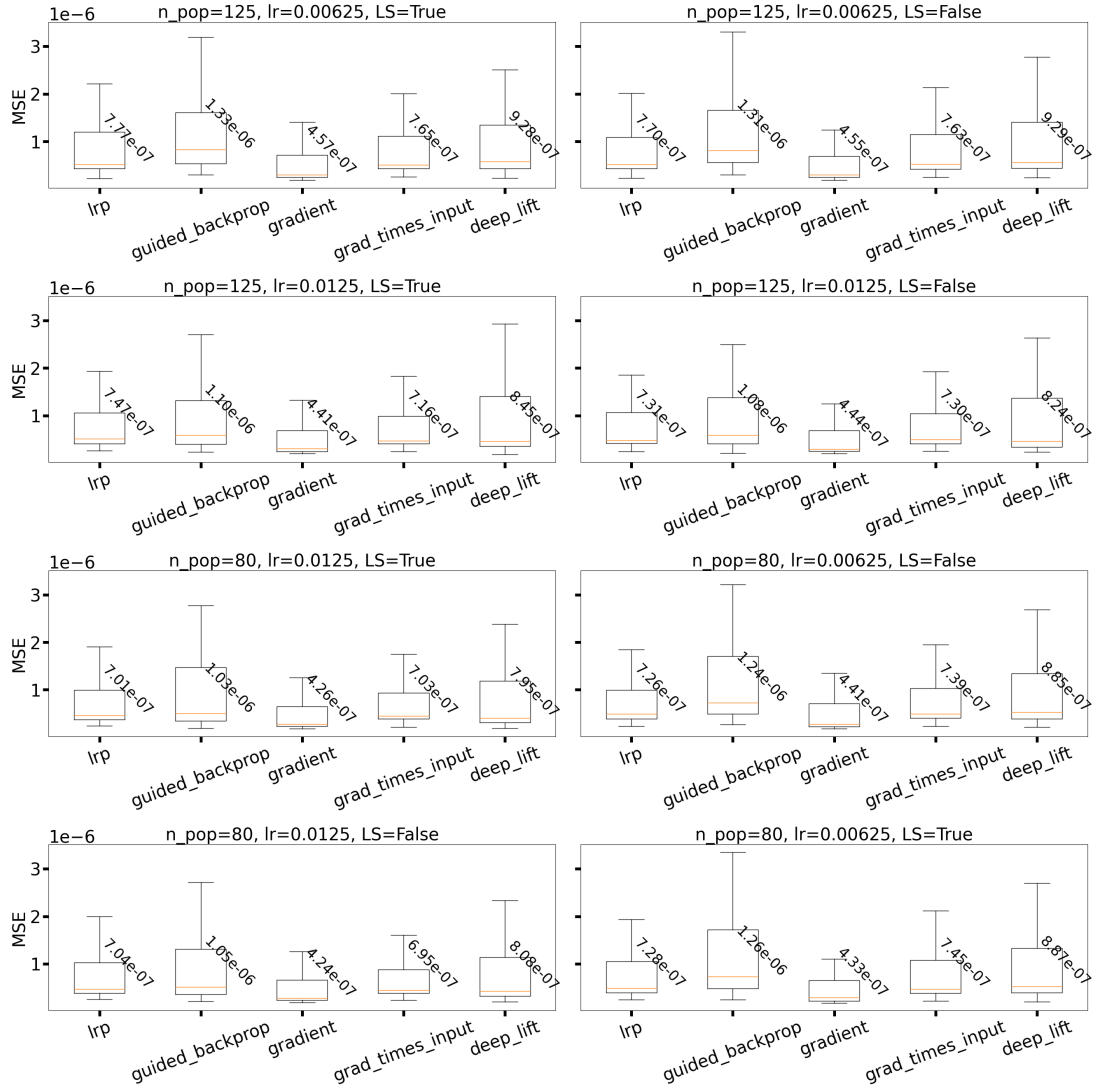


Figure 14: Similarity in terms of MSE between target explanation map, $g(x_{target})$, and best final adversarial explanation map, $g(x_{adv})$, for 8 different hyperparameter configurations. Dataset: CIFAR100. Model: VGG16. The Gradient XAI method is the most susceptible to attacks while Guided backpropagation and Deep Lift are the hardest to attack; LRP and Gradient x Input are similar.

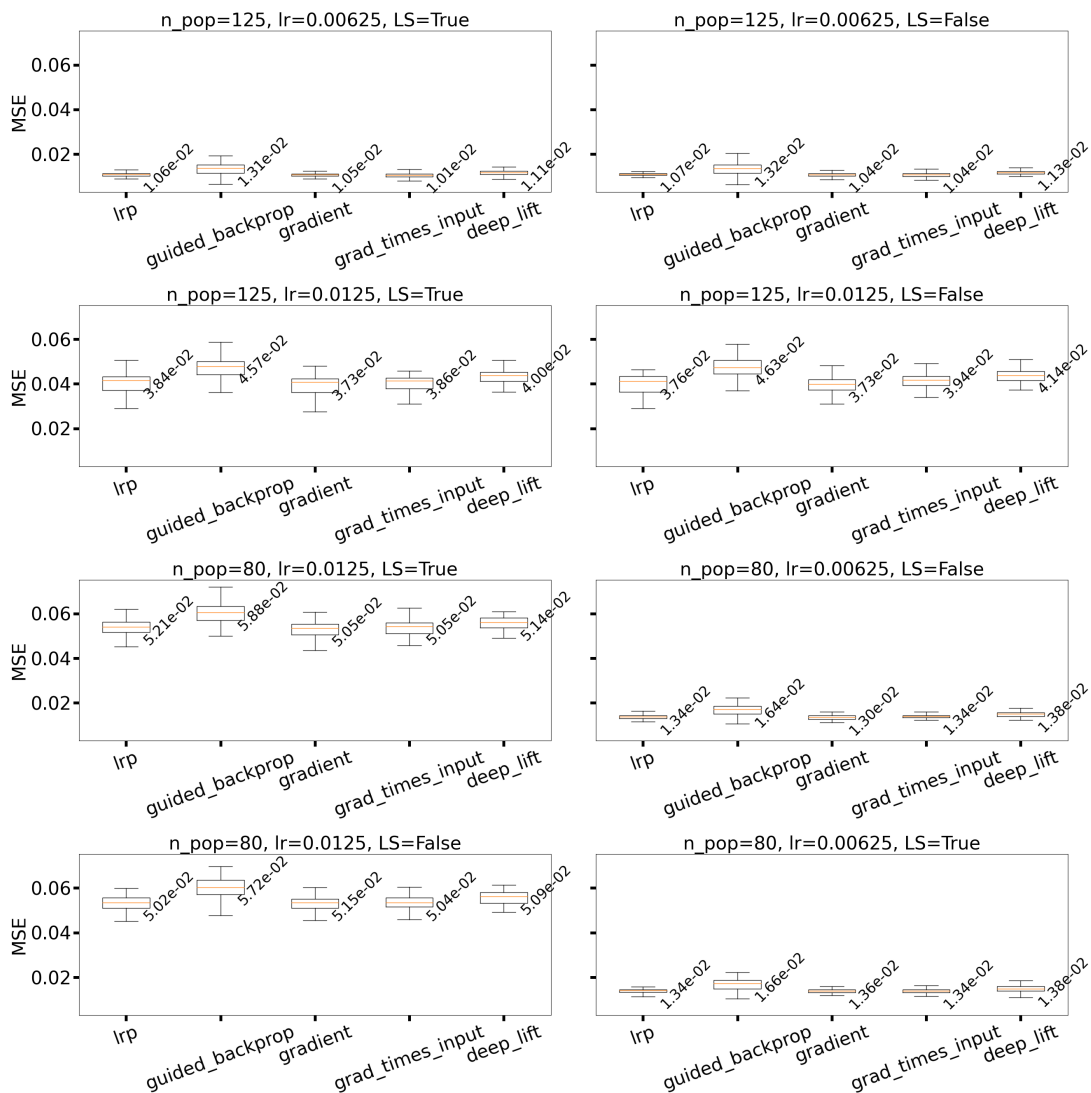


Figure 15: MSE loss value for input image versus chosen adversarial image for 8 different hyperparameter configurations. Dataset: CIFAR100. Model: VGG16. A higher learning rate and a smaller population size (i.e., more gradient steps) contribute to the perturbation of the image. The sampling method has no effect.

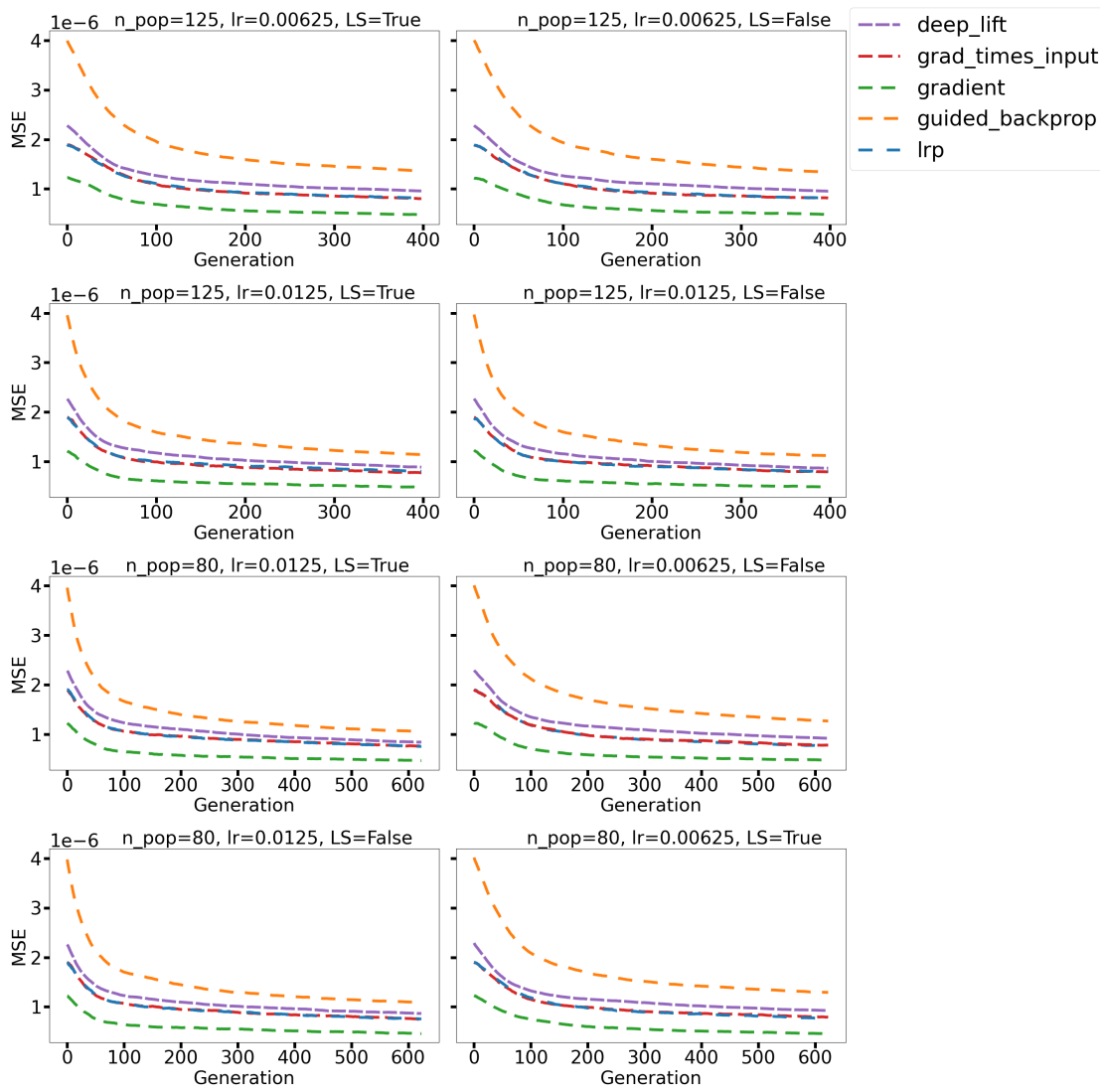


Figure 16: MSE loss value as function of evolutionary generation for 8 different hyperparameter configurations. Dataset: CIFAR100. Model: VGG16.

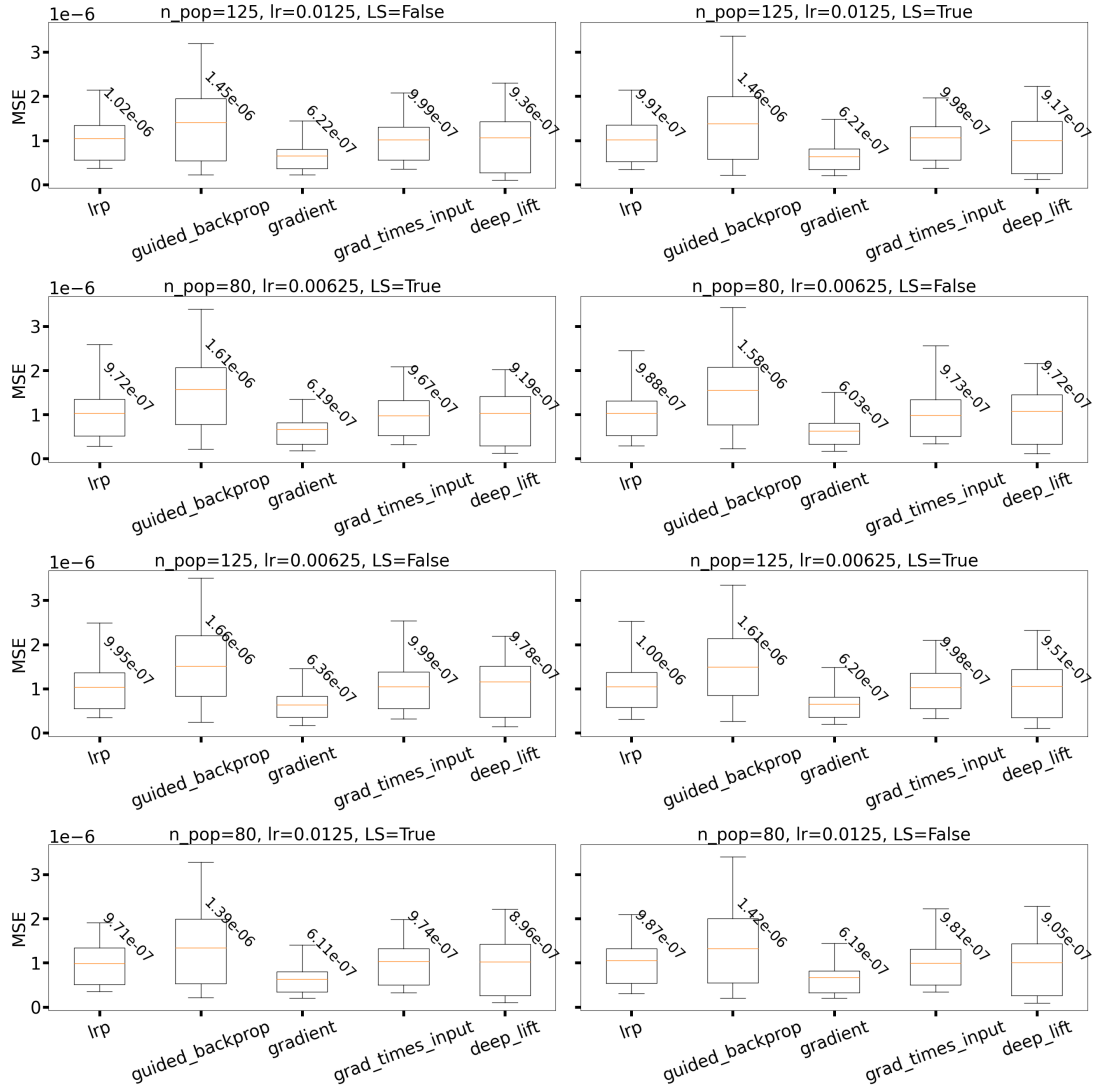


Figure 17: Similarity in terms of MSE between target explanation map, $g(x_{target})$, and best final adversarial explanation map, $g(x_{adv})$, for 8 different hyperparameter configurations. Dataset: CIFAR100. Model: MobileNet. The Gradient XAI method is the most susceptible to attacks while Guided backpropagation is the hardest to attack; Deep Lift, LRP, and Gradient x Input are similar.

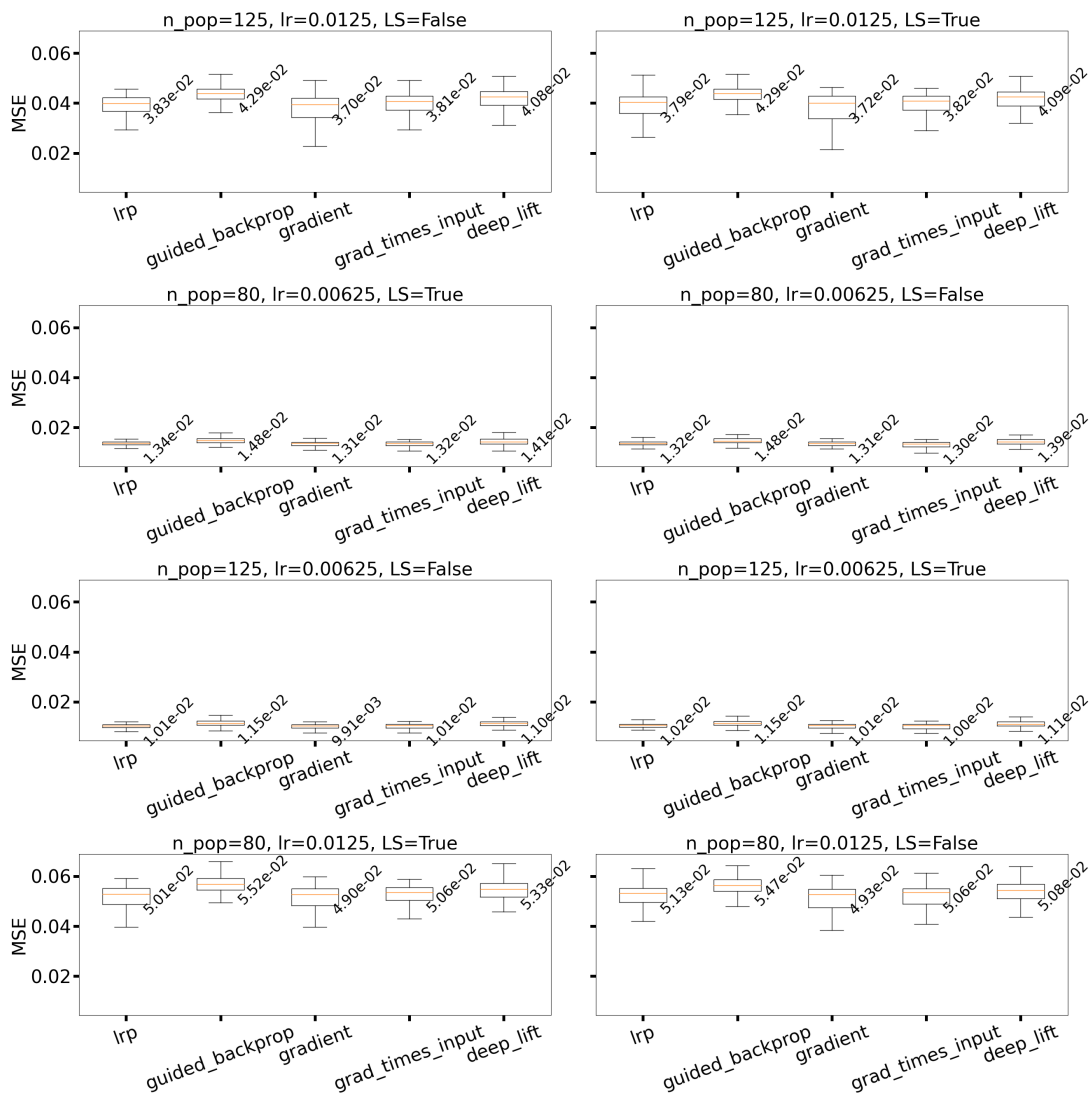


Figure 18: MSE loss value for input image versus chosen adversarial image for 8 different hyperparameter configurations. Dataset: CIFAR100. Model: MobileNet. A higher learning rate and a smaller population size (i.e., more gradient steps) contribute to the perturbation of the image. The sampling method has no effect.

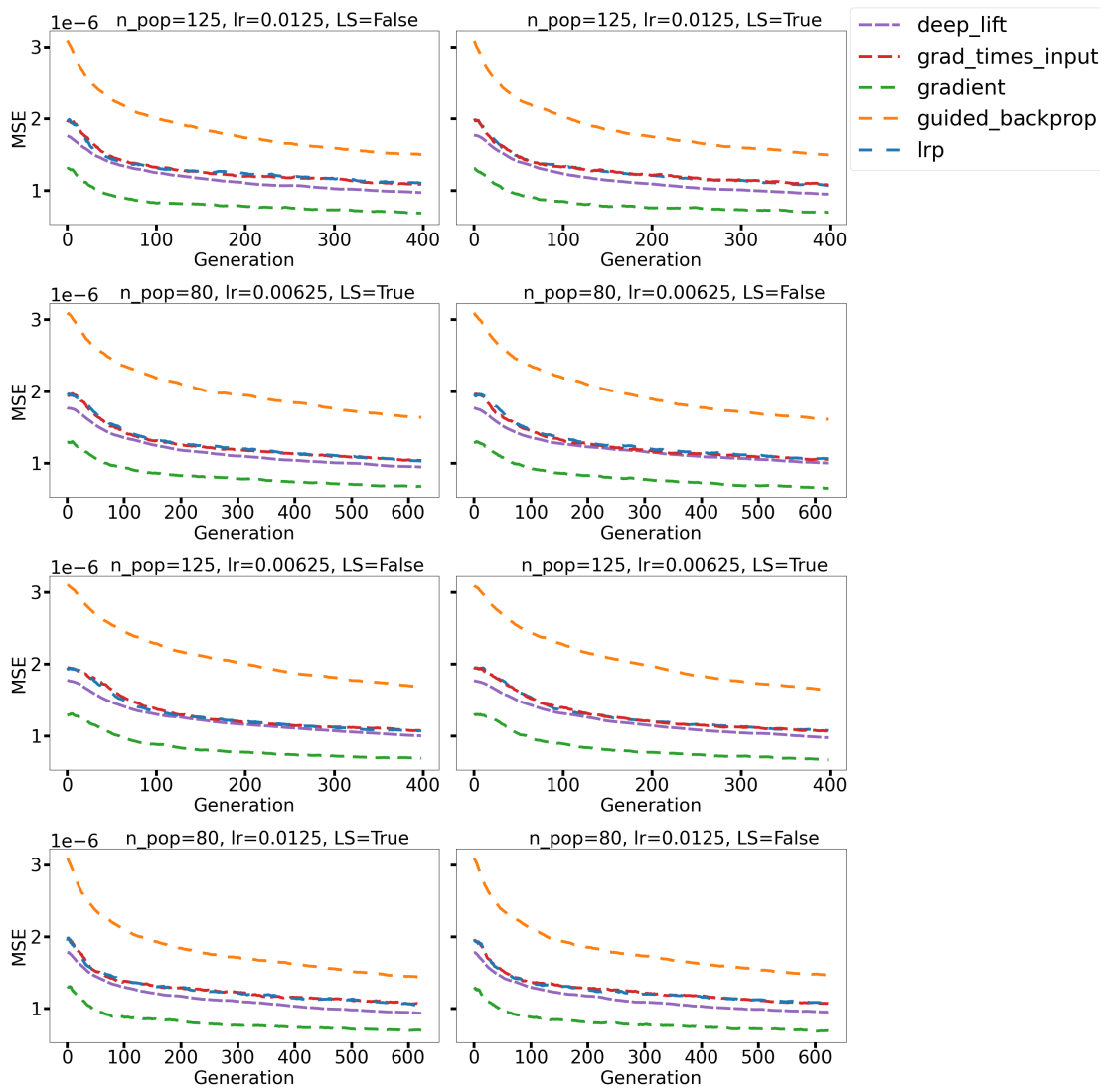


Figure 19: MSE loss value as function of evolutionary generation for 8 different hyperparameter configurations. Dataset: CIFAR100. Model: MobileNet.